ISSN 1674-1056
http://cpb.iphy.ac.cn
http://iopscience.iop.org/cpb
中国物理 B
Chinese Physics
中国物理 Chinese Physics B

Electronic structure of molecular beam epitaxy grown 1T'-$MoTe_2$ film and strain effect

Xue Zhou(周雪)[1], Zeyu Jiang(姜泽禹)[1], Kenan Zhang(张柯楠)[1], Wei Yao(姚维)[1], Mingzhe Yan(颜明哲)[1], Hongyun Zhang(张红云)[1], Wenhui Duan(段文晖)[1], Shuyun Zhou(周树云)[1,2]

Citation: Chin. Phys. B . 2019, 28(10): 107307 . **doi:** 10.1088/1674-1056/ab43ba
Journal homepage: http://cpb.iphy.ac.cn; http://iopscience.iop.org/cpb

What follows is a list of articles you may be interested in

Quantum spin Hall and quantum valley Hall effects in trilayer graphene and their topological structures

Majeed Ur Rehman, A A Abid

Chin. Phys. B . 2017, 26(12): 127304 . **doi:** 10.1088/1674-1056/26/12/127304

Quantum anomalous Hall effect in real materials

Jiayong Zhang(张加永), Bao Zhao(赵宝), Tong Zhou(周通), Zhongqin Yang(杨中芹)

Chin. Phys. B . 2016, 25(11): 117308 . **doi:** 10.1088/1674-1056/25/11/117308

Transport properties of the topological Kondo insulator SmB_6 under the irradiation of light

Guo-Bao Zhu(朱国宝), Hui-Min Yang(杨慧敏)

Chin. Phys. B . 2016, 25(10): 107303 . **doi:** 10.1088/1674-1056/25/10/107303

The robustness of quantum spin Hall effect to the thickness fluctuation in HgTe quantum wells

Guo Huai-Ming, Zhang Xiang-Lin, Feng Shi-Ping

Chin. Phys. B . 2012, 21(11): 117301 . **doi:** 10.1088/1674-1056/21/11/117301

Quantum spin Hall effect in a square-lattice model under a uniform magnetic field

Guo Huai-Ming, Feng Shi-Ping

Chin. Phys. B . 2012, 21(7): 077303 . **doi:** 10.1088/1674-1056/21/7/077303

RAPID COMMUNICATION

Electronic structure of molecular beam epitaxy grown 1T′-$MoTe_2$ film and strain effect*

Xue Zhou(周雪)[1], Zeyu Jiang(姜泽禹)[1], Kenan Zhang(张柯楠)[1], Wei Yao(姚维)[1], Mingzhe Yan(颜明哲)[1], Hongyun Zhang(张红云)[1], Wenhui Duan(段文晖)[1], and Shuyun Zhou(周树云)[1,2,†]

[1] *State Key Laboratory of Low Dimensional Quantum Physics and Department of Physics, Tsinghua University, Beijing* 100084, *China*
[2] *Collaborative Innovation Center of Quantum Matter, Beijing* 100084, *China*

(Received 18 June 2019; revised manuscript received 6 September 2019; published online 30 September 2019)

Atomically thin transition metal dichalcogenide films with distorted trigonal (1T′) phase have been predicted to be candidates for realizing quantum spin Hall effect. Growth of 1T′ film and experimental investigation of its electronic structure are critical. Here we report the electronic structure of 1T′-$MoTe_2$ films grown by molecular beam epitaxy (MBE). Growth of the 1T′-$MoTe_2$ film depends critically on the substrate temperature, and successful growth of the film is indicated by streaky stripes in the reflection high energy electron diffraction (RHEED) and sharp diffraction spots in the low energy electron diffraction (LEED). Angle-resolved photoemission spectroscopy (ARPES) measurements reveal a metallic behavior in the as-grown film with an overlap between the conduction and valence bands. First principles calculation suggests that a suitable tensile strain along the *a*-axis direction is needed to induce a gap to make it an insulator. Our work not only reports the electronic structure of MBE grown 1T′-$MoTe_2$ films, but also provides insights for strain engineering to make it possible for quantum spin Hall effect.

Keywords: quantum spin Hall effect, 1T′-$MoTe_2$, molecular beam epitaxy (MBE), transition metal dichalcogenides (TMDCs)

PACS: 73.43.–f, 81.15.Hi, 71.15.–m, 68.65.–k **DOI:** 10.1088/1674-1056/ab43ba

1. Introduction

Topological materials have provided an important platform for exploring new physics and realizing novel quantum phenomena.[1,2] For example, quantum spin Hall effect (QSHE)[3–5] is expected in two-dimensional topological insulators.[6] Transition metal dichalcogenides (TMDCs) with distorted trigonal structure (1T′) have been predicted to be important candidates for realizing QSHE with potential applications in topological field effect transistors.[7–11] Recently, 1T′-WTe_2 thin films have been revealed to show electronic properties compatible with QSHE.[12–14] 1T′-$MoTe_2$ has similar crystal structure to 1T′-WTe_2[15] and can also be a potential candidate for QSHE. $MoTe_2$ crystalizes in three structures, hexagonal (2H), monoclinic (1T′),[15] and orthorhombic (T_d).[16] Bulk single crystal of 1T′-$MoTe_2$ undergoes a phase transition to T_d phase[16] which hosts type-II Weyl fermions,[17–19] and a superconducting transition has been reported at even lower temperature,[20] however, mechanically exfoliated few layered 1T′-$MoTe_2$ has been reported to be a semiconductor.[15]

While growth of 1T′-$MoTe_2$ thin film by chemical vapor deposition has been reported,[21–25] molecular beam epitaxy (MBE) growth of 1T′-$MoTe_2$ films under ultra-high vacuum has the advantage of being directly compatible with the *in situ* electronic structure measurement by angle-resolved photoemission spectroscopy (ARPES). So far, despite extensive efforts, molecular beam epitaxy growth of atomically thin 1T′-$MoTe_2$ films[26–29] has been challenging due to the existence of another stable phase 2H-$MoTe_2$,[30] which often leads to a mixture of both 1T′ and 2H phases in the as-grown $MoTe_2$ films.[26–28] Here we report the successful growth of 1T′-$MoTe_2$ films at the optimum growth condition after a systematic study of the film growth at different substrate temperatures. ARPES measurements show that the as-grown film shows a metallic behavior with an overlap between the conduction and valence bands. First principles calculation suggests that a 3% tensile uniaxial strain along the *a*-axis direction is needed to induce a significant gap to be compatible with QSHE.

2. Methods

The 1T′-$MoTe_2$ films were grown on bilayer graphene/6H-SiC(0001) by MBE. The 6H-SiC(0001) substrate was degassed at 650 °C and annealed from 650 °C to 1350 °C for 60 cycles to form bilayer graphene films on the top surface.[31] High purity Mo (99.99% purity) and Te (99.999% purity) were then evaporated through an e-beam evaporator and Knudsen cell respectively with a flux ratio of ∼ 1 : 20.

*Project supported by the National Basic Research Program of China (Grant Nos. 2016YFA0301004 and 2015CB921001) and the National Natural Science Foundation of China (Grant Nos. 11334006, 11725418, and 11674188).

†Corresponding author. E-mail: syzhou@mail.tsinghua.edu.cn

© 2019 Chinese Physical Society and IOP Publishing Ltd

The growth process was monitored by *in situ* reflection high energy electron diffraction (RHEED) and low energy electron diffraction (LEED). ARPES measurements were performed *in situ* with a helium lamp source at a temperature of ~ 10 K under ultra-high vacuum.

The density functional theory (DFT) calculations are performed using the Vienna *ab initio* simulation package (VASP)[32] with the Perdew–Burke–Ernzerhof (PBE)[33] exchange–correlation functional and a plane wave energy cutoff of 500 eV. A k-point grid of $16 \times 20 \times 1$ is applied to sample the Brillouin zone. The pristine geometric structure of the monolayer is fully relaxed until the residual forces on each atom are less than 0.001 eV/Å, and the obtained equilibrium lattice parameters are $a = 3.475$ Å and $b = 6.367$ Å. To simulate the uniaxial strain along the a-axis (b-axis), a stain is applied along the a-axis (b-axis), and the length of b-axis (a-axis) as well as the ionic positions is optimized until the residual forces are less than 0.001 eV/Å. The spin–orbit coupling (SOC) effect has been taken into account in our calculations.

3. Results and discussion

Figures 1(a) and 1(b) show the top and side views of the crystal structure of 1T′-$MoTe_2$. The Mo atoms deviate from the center of the octahedron formed by six Te atoms, forming zigzag Mo chains along the a-axis direction (see the top view in Fig. 1(a)) and distorted Te octahedra in the b–c plane (side view in Fig. 1(b)). Graphene is a fantastic substrate for growing films with different crystal structures and symmetries through van der Waals epitaxiy,[34] and is used as the substrate for growing 1T′-$MoTe_2$ film. Figures 1(c) and 1(d) show the RHEED and LEED patterns of the graphene/SiC substrate. Figures 1(e) and 1(f) show the RHEED and LEED patterns of the 1T′-$MoTe_2$ films under optimum growth conditions. Sharp streaky stripes (indicated by yellow arrow in Fig. 1(e)) and six diffraction spots (Fig. 1(f)) from the 1T′-$MoTe_2$ film are observed in the RHEED and LEED patterns, respectively. The 1T′-$MoTe_2$ film grows mainly along the same orientation as the graphene substrate with a small distribution of azimuthal angles in the LEED pattern due to the weak van der Waals growth with weak coupling between the 1T′-$MoTe_2$ film and graphene. Because of the different crystal symmetries between the substrate (three-fold symmetry) and the 1T′-$MoTe_2$ film (two-fold symmetry), there are three equivalent orientations of 1T′-$MoTe_2$ films on graphene, leading to apparently hexagonal LEED patterns, similar to the case of 1T′-WTe_2 film[12] and the previous report on 1T′-$MoTe_2$[29] yet with better LEED pattern. The observation of diffraction spots from both the 1T′-$MoTe_2$ film and the graphene substrate suggests that the 1T′-$MoTe_2$ film is atomically thin, ~ 1 monolayer (ML) thick. Increasing the growth time leads to weaker diffraction spots from the substrate and the graphene diffraction spots disappear at 2 ML (see Appendix A), however, no major change in the electronic structure is observed since the difference in the electronic structure of monolayer, bilayer, and multilayer 1T′-$MoTe_2$ films is small due to the small band splitting. Using the lattice constants of graphene as a reference, the extracted in-plane lattice constants of 1T′-$MoTe_2$ from the LEED pattern are $a = 3.47$ Å and $b = 6.48$ Å, suggesting a 2% (tensile) strain along the b-axis direction compared to the lattice constants of $a = 3.48$ Å and $b = 6.33$ Å in the bulk crystal.[15]

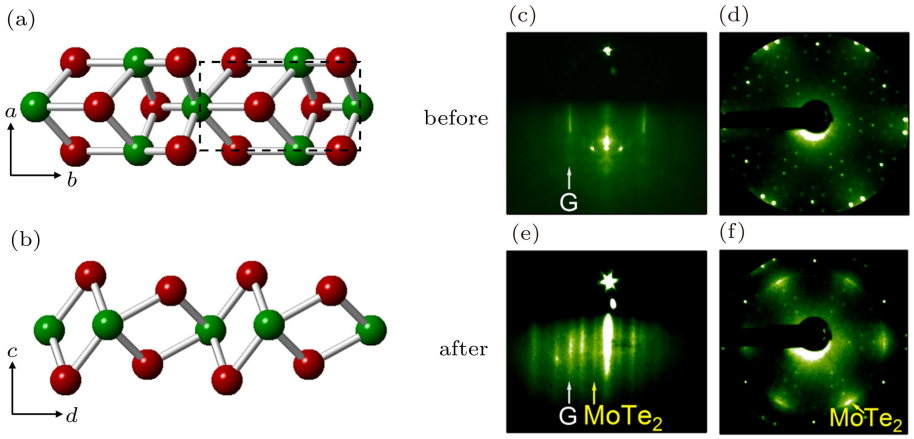


Fig. 1. Crystal structure of 1T′-$MoTe_2$ and diffraction patterns from RHEED and LEED. (a) and (b) Top and side views of the crystal structure of 1T′-$MoTe_2$. Red and green balls represent Te and Mo atoms, respectively. The dashed box indicates the unit cell. RHEED patterns of (c) the graphene/SiC substrates and (e) the as-grown 1T′-$MoTe_2$ sample. LEED patterns of (d) the graphene/SiC substrates and (f) the as-grown 1T′-$MoTe_2$ sample measured at a beam energy of 120 eV. The white and yellow arrows indicate the patterns from graphene and 1T′-$MoTe_2$, respectively.

The growth condition is critically dependent on the substrate temperature. Figure 2 shows a systematic study of the RHEED and LEED patterns of the films grown at different substrate temperatures while maintaining other experimental conditions fixed. When the substrate temperature is 331 °C, no detectable signals from $MoTe_2$ are observed in the RHEED (Fig. 2(a)) or LEED patterns (Fig. 2(e)). Only in a small temperature window of ~ 25 °C between 338 °C and 363 °C,

streaky stripes can be observed (indicated by the yellow arrows) in RHEED (Figs. 2(b)–2(d)) and diffraction spots are observed in the LEED patterns (Figs. 2(f)–2(h)). The sharpest streaky stripes from the RHEED pattern (Fig. 2(c)) and the best signal from the LEED pattern (Fig. 2(g)) obtained at the substrate temperature of 350 °C indicate that the optimum growth condition includes the substrate temperature of 350 °C.

Although bulk crystal of 1T′-$MoTe_2$ is quite stable in air, atomically thin 1T′-$MoTe_2$ films have been reported to be very sensitive to air.[23,26,30,35,36] Therefore *ex situ* atomic force microscopy (AFM) and Raman characterizations of the films are not practical. Direct experimental electronic structure of the as-grown film by *in situ* ARPES measurements can provide direct evidence for the 1T′-$MoTe_2$ film, and moreover, provide insights for evaluating its compatability with QSHE.

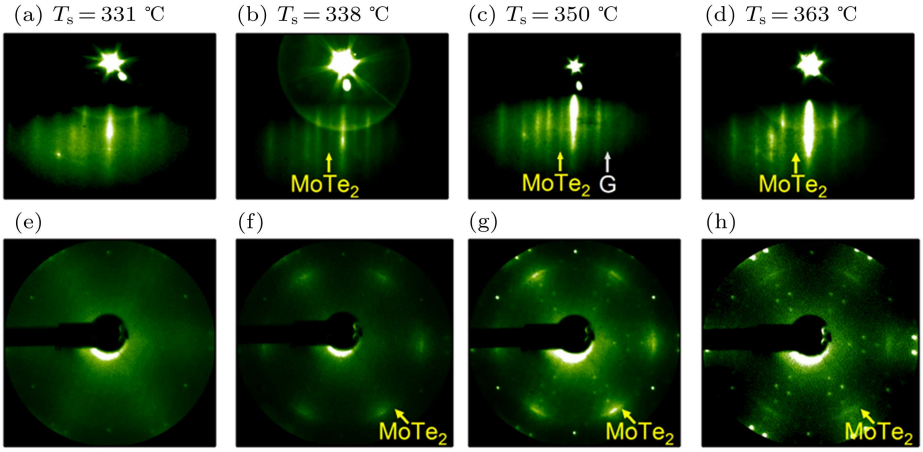


Fig. 2. RHEED and LEED patterns for films grown at different substrate temperatures. (a)–(d) RHEED patterns after growing at the substrate temperature of 331 °C, 338 °C, 350 °C, and 363 °C, respectively. (e)–(h) Corresponding LEED patterns. The yellow and white arrows indicate diffraction spots from 1T′-$MoTe_2$ and graphene, respectively.

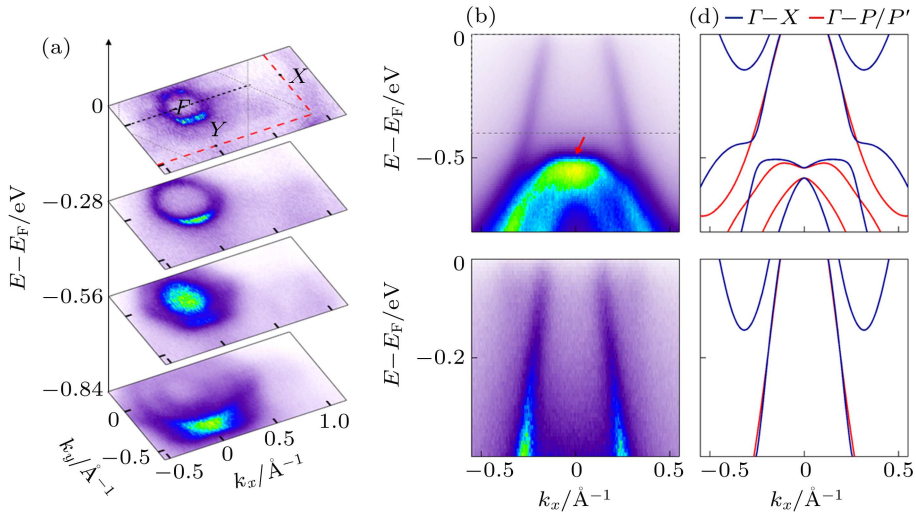


Fig. 3. Electronic structure of 1T′-$MoTe_2$ revealed by ARPES measured at ∼ 10 K. (a) Intensity maps measured from E_F to −0.84 eV with an integrated energy window of 50 meV. (b) ARPES spectrum measured along the Γ–X direction (marked by dotted line in (a)). (c) Zoom-in dispersion near E_F. (d) Calculated dispersions along the Γ–X direction (blue) and Γ–P/P' (red) and (e) zoom-in dispersion near E_F with a uniaxial strain of 2% along the b-axis direction and a shift −0.09 eV in energy.

Figure 3 shows the electronic structure of 1T′-$MoTe_2$ revealed by *in situ* ARPES measurements. Figure 3(a) shows the intensity maps measured from E_F to −0.84 eV. Since the 2H-$MoTe_2$ is a semiconductor with a gap of larger than 1 eV,[37] this confirms that the measured band dispersion is not from the 2H-$MoTe_2$ but from the 1T′-$MoTe_2$. A hexagonal pocket centered at the Γ point is observed at E_F and its size increases at low energies, suggesting that it is a hole pocket. Below −0.56 eV, a new pocket emerges at the Γ point and further splits into two circular pockets, resulting in three hole pockets in total at −0.84 eV. Figure 3(b) shows the dispersions measured along the Γ–X direction. The dispersion shows a linear dispersing hole pocket through E_F and two parabolic bands below −0.56 eV, consistent with the intensity maps in Fig. 3(a). Figure 3(c) shows a zoom-in of the dispersion near E_F. In addition to the hole pocket near E_F as discussed above, there is another dispersing band within −0.15 eV, suggesting that this is likely the electron pocket from the conduction band. Figures 3(d) and 3(e) show the calculated band dispersion for comparison.[12] By using the extracted experimental lattice

constant from LEED, which indicates a strain of 2% (tensile) along the *b*-axis direction, a good agreement with the experimental results is obtained. The overall band structure is similar to that of 1T′-WTe_2,[12,38] yet with two major differences. Firstly, the two bands below −0.56 eV almost cross (pointed by the red arrow in Fig. 3(b)), which is different from those in the 1T′-WTe_2 film and is not discussed in previous work on 1T′-$MoTe_2$.[12] Indeed, the better agreement between the ARPES data and the calculated band structure of the strained film compared to the calculated result of the unstrained film in previous work[12] also indicates the important role of stain in this material. Secondly, both the experimental and calculated results reveal an overlap between the conduction and valence bands, while doped 1T′-WTe_2 has been reported to be an insulator with a gap of 45 meV.[12] Therefore, our ARPES data and calculation show that different from 1T′-WTe_2, the as-grown 1T′-$MoTe_2$ film is metallic with an overlap between the valence and conduction bands.

Since the electronic structures of 1T′-$MoTe_2$ films[7] and bulk crystals[39–41] are strongly dependent on the strain, we calculate the evolution of the electronic structure with uniaxial strain to provide more insights. Figure 4 shows the calculated band structure of monolayer 1T′-$MoTe_2$ film under uniaxial strain along the *b*-axis (Figs. 4(a)–4(e)) and *a*-axis (Figs. 4(f)–4(j)) with strains ranging from −2% to 3%. The application of a tensile strain along the *a*-axis direction has similar effect to the application of a compressive strain along the *b*-axis direction. The uniaxial strain has two major effects. Firstly, it changes the splitting of the two bands below −0.5 eV at the Γ point. More importantly, it changes the energy position of these valence bands significantly, while maintaining the energy position of the conduction band. By applying a tensile strain along the *a*-axis, the overlap between the valence and conduction bands decreases, until eventually a gap of 47 meV emerges at 3% strain (Fig. 4(j)). The opening of such a band gap is critical, since it makes 1T′-$MoTe_2$ potentially a quantum spin Hall insulator if the Fermi energy is further tuned to inside the gap region. Therefore in order to realize QSHE in 1T′-$MoTe_2$ films, a tensile strain (3%) along the *a*-axis is needed.

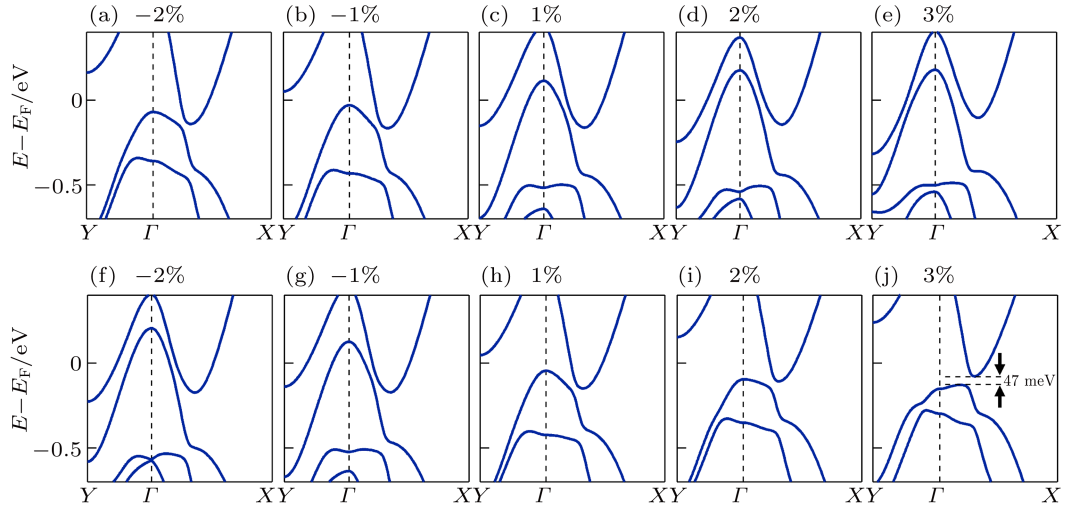


Fig. 4. Evolution of the electronic structure with strain from first principles calculation. (a)–(e) Calculated band structure of monolayer 1T′-$MoTe_2$ with uniaxial strains from −2% to 3% along the *b*-axis direction. (f)–(j) Calculated band structure of monolayer 1T′-$MoTe_2$ with uniaxial strains from −2% to 3% along the *a*-axis direction. All calculated dispersions are shifted by −0.09 eV in energy.

4. Conclusion

To summarize, we have successfully grown high-quality atomically thin 1T′-$MoTe_2$ films using MBE after a systematic investigation of the growth at different substrate temperatures, which is confirmed by RHEED, LEED, and ARPES measurements. Furthermore, ARPES measurements show that the as-grown film is a metal with an overlap between the conduction and valence bands, which is attributed to the strain effect. Comparison of calculated band structures at different strains further suggests that a suitable tensile strain (3% tensile strain along the *a*-axis direction) can induce a significant gap between the conduction and valence bands. Our work not only reports the MBE growth conditions for obtaining 1T′-$MoTe_2$ thin film and its experimental electronic structure, but also provides insights for band structure engineering of 1T′-$MoTe_2$ film to make it a quantum spin Hall insulator.

Appendix A: Supplemental material

Figure A1 shows a comparison of RHEED, LEED, and calculated electronic structure for 1 ML and 2 ML films. The observation of graphene spots in Fig. A1(b) shows that the sample is ∼ 1 ML. By doubling the growth time, the diffraction spots from graphene disappear. A comparison of the electronic structures for 1 ML and 2 ML shows that the splitting is very weak and beyond the resolution of the ARPES experiments.

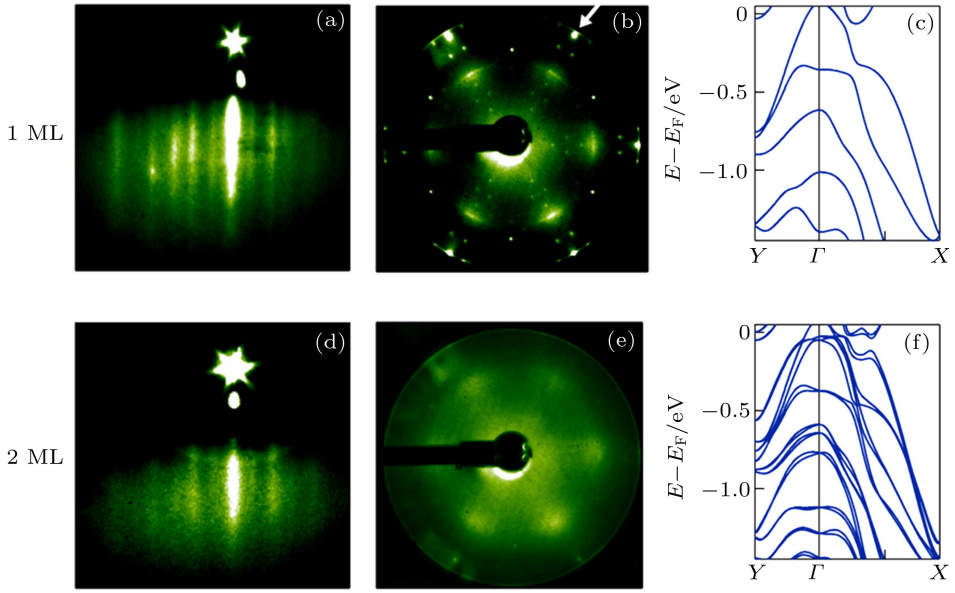


Fig. A1. Comparison of RHEED, LEED, and calculated electronic structure for 1 ML and 2 ML films. (a)–(c) RHEED, LEED, and calculated electronic structure of 1 ML film, white arrow in (b) indicates the patterns from graphene. (d)–(f) RHEED, LEED, and calculated electronic structure of 2 ML film.

References

[1] Hasan M Z and Kane C L 2010 *Rev. Mod. Phys.* **82** 3045
[2] Qi X L and Zhang S C 2011 *Rev. Mod. Phys.* **83** 1057
[3] Bernevig B A, Hughes T L and Zhang S C 2006 *Science* **314** 1757
[4] König M, Wiedmann S, Brüne C, Roth A, Buhmann H, Molenkamp L W, Qi X L and Zhang S C 2007 *Science* **318** 766
[5] Liu C X, Hughes T L, Qi X L, Wang K and Zhang S C 2008 *Phys. Rev. Lett.* **100** 236601
[6] Kane C L and Mele E J 2005 *Phys. Rev. Lett.* **95** 226801
[7] Qian X F, Li J W, Fu L and Li J 2014 *Science* **346** 1344
[8] Guo H, Zhang X and Shiping F 2012 *Chin. Phys. B* **21** 117301
[9] Rehman M U and Abid A A 2017 *Chin. Phys. B* **26** 127304
[10] Wang X, Li P and Ran Zhao Luo W 2018 *Chin. Phys. B* **27** 087305
[11] Shen D P, Zhang X D, Sun Y, Kang T T, Dai N and Chu Jun Haoand Yu G L 2017 *Acta Phys. Sin.* **66** 247301 (in Chinese)
[12] Tang S J, Zhang C F, Wong D, *et al.* 2017 *Nat. Phys.* **13** 683
[13] Fei Z Y, Palomaki T, Wu S F, Zhao W J, Cai X H, Sun B S, Nguyen P, Finney J, Xu X D and Cobden D H 2017 *Nat. Phys.* **13** 677
[14] Wu S F, Fatemi V, Gibson Q D, Watanabe K, Taniguchi T, Cava R J and Jarillo-Herrero P 2018 *Science* **359** 76
[15] Keum D H, Cho S, Kim J H, Choe D H, Sung H J, Kan M, Kang H, Hwang J Y, Kim S W, Yang H, Chang K J and Lee Y H 2015 *Nat. Phys.* **11** 482
[16] Zhang K N, Bao C H, Gu Q Q, Ren X, Zhang H X , Deng K, Wu Y, Li Y, Feng J and Zhou S Y 2016 *Nat. Commun.* **7** 13552
[17] Soluyanov A A, Gresch D, Wang Z, Wu Q, Troyer M, Dai X and Bernevig B A 2015 *Nature* **527** 495
[18] Deng K, Wan G L, Deng P, Zhang K N, Ding S J, Wang E Y, Yan M Z, Huang H Q, Zhang H Y, Xu Z L, Denlinger J, Fedorov A, Yang H T, Duan W H, Fan S S, Zhang H J, Chen X and Zhou S Y 2016 *Nat. Phys.* **12** 1105
[19] Huang L, McCormick T M, Masayuki O, Zhao Z, Suzuki M T, Arita R, Wu Y, Mou D X, Cao H B, Yan J Q, Trivedi N and Kaminski A 2016 *Nat. Mater.* **1** 1155
[20] Qi Y P, Naumov P G, Ali M N, Rajamathi C R, Schnelle W, Barkalov O, Hanfland M, Wu S C, Shekhar C, Sun Y, Süß V, Schmidt M, Schwarz U, Felser C, Yan B H and Medvedev S A 2016 *Nat. Commun.* **7** 11038
[21] Park J C, Yun S J, Kim H, Park J H, Chae S H, An S J, Kim J G, Kim S M, Kim K K and Lee Y H 2015 *Acs Nano* **9** 6548
[22] Zhou L, Zubair A, Wang Z, Zhang X, Ouyang F P, Xu K, Fang W J, Ueno K, Li J, Palacios T, Kong J and Dresselhaus M S 2016 *Adv. Mater.* **28** 9526
[23] Naylor C H, Parkin W M, Ping J L, Gao Z L, Zhou Y R, Kim Y, Streller F, Carpick R W, Rappe A M, Drndić M and Kikkawa J M 2016 *Nano Lett.* **16** 4297
[24] Han G H, Keum D, Zhao J, Shin B G, Song S, Bae J J, Lee J, Kim J H, Moon B H and Lee Y H 2016 *2D Mater.* **2** 031010
[25] Zhou J D, Liu F C, Lin J H, Huang X W, Xia J, Zhang B W, Zeng Q S, Wang H, Zhu C, Niu L, Wang X W, Fu W, Yu P, Chang T R, Hsu C H, Wu D, Jeng H T, Huang Y Z, Lin H, Shen Z X, Yang C L, Lu L, Suenaga K, Zhou W, Pantelides S T, Liu G T and Liu Z 2016 *Adv. Mater.* **29** 1603471
[26] Chen J L, Wang G Y, Tang Y, Tian H, Xu J P, Dai X Q, Xu H, Jia J F, Wingkin H and Xie M H 2017 *ACS Nano* **11** 3282
[27] Yu Y, Wang G, Qin S, Wu N, Wang Z, He K and Zhang X A 2017 *Carbon* **115** 526
[28] Vishwanath S, Sundar A, Liu X Y, Azcatl A, Lochocki E, Woll A R, Rouvimov S, Hwang W S, Lu N, Peng X, Lien H H, Weisenberger J, McDonnell S, Kim M J, Dobrowolska M, Furdyna J K, Shen K, Wallace R M, Jena D and Xing H G 2017 *J. Cryst. Growth* **482** 61
[29] Tang S J, Zhang C F, Jia C J, Ryu H, Hwang C, Hashimoto M, Lu D H, Liu Z, Devereaux T P, Shen Z X and Mo S K 2018 *APL Mater.* **6** 026601
[30] Diaz H C, Chaghi R, Ma Y J and Batzill M 2015 *2D Mater.* **2** 040010
[31] Wang Q Y, Zhang W H, Wang L L, He K, Ma X C and Xue Q K 2013 *J. Phys.: Condens. Matter* **25**
[32] Kresse G and Furthmüller J 1996 *Phys. Rev. B* **54** 11169
[33] Perdew J P, Burke K and Ernzerhof M 1996 *Phys. Rev. Lett.* **77** 3865
[34] Koma A, Sunouchi K and Miyajima T 1984 *J. Vac. Sci. Technol. B* **3** 724
[35] Sun Y F, Wang Y X, Sun D, Carvalho B R, Read C G, Lee C h, Lin Z, Fujisawa K, Robinson J A, Crespi V H, Terrones M and Schaak R E 2016 *Angew. Chem. Int. Ed.* **55** 2830
[36] Ruppert C, Aslan O B and Heinz T F 2014 *Nano Lett.* **11** 6231
[37] Zhang H Y, Bao C H, Jiang Z Y, Zhang K N, Li H, Chen C Y, Wu Y, Duan W H, Asensio M C and Zhou S Y 2018 *Nano Lett.* **18** 4664
[38] Zheng F P, Cai C Y, Ge S F, Zhang X F, Liu X, Lu H, Zhang Y D, Qiu J, Taniguchi T, Watanabe K, Jia S, Qi J S, Chen J H, Sun D and Feng J 2016 *Adv. Mater.* **28** 4845
[39] Yang J J, Colen J, Liu J, Nguyen M C, Chern G W and Louca D 2017 *Sci. Adv.* **3** eaao4949
[40] Kim H J, Kang S H, Hamada I and Son Y W 2017 *Phys. Rev. B* **95** 180101
[41] Dai X, Le C, Wu X X and Qin S S 2016 *Chin. Phys. Lett.* **33** 127301